Chapter 5

Significance of nanoparticle shape on stagnation-point flow in the presence of induced magnetic field *

5.1 Introduction

The nanoparticles can be categorized into spherical and non-spherical nanoparticles based on their physical shape. Different shaped nanoparticle exhibits different properties and different heat transfer capabilities. Non-spherical nanoparticles have gained popularity for their ability in changing the thermophysical properties of a nanofluid. Blood is a connective tissue in fluid form. Blood flow utilizing nanoparticles are important in the medical industry for cancer treatment and drug delivery. Induced magnetic field paired with blood flow plays a decisive role in blood pumps, treatment of cardiac diseases and has many other biomedical applications. The significance of multiple slip and nanoparticle shape on stagnation point flow of blood-based silver nanofluid considering chemical reaction, induced magnetic field, thermal radiation, and linear heat source which is beneficial in cancer therapy, biomedical imaging, hyperthermia, and tumor therapy is investigated. Relevant similarity transformations are effectuated in converting the mathematically modelled governing equations into a system of ODEs and are then numerically resolved in MATLAB employing the adaptive Runge-Kutta method and the Newton Raphson method. Observations on the consequence of differing parameters on varying attributes are achieved via tables and graphs. Additionally, the shape effect of nanoparticles on various attributes is also evaluated. The current chapter makes

*Published in: Surfaces and Interfaces (Elsevier), 2021; 25; 101267.

an attempt in answering the following research questions:

- What is the significance of thermal slip and solutal slip parameters on the nanofluid temperature and nanofluid concentration, respectively?
- How does the nanoparticle shape affect the flow profiles?
- What is the variation in the nanofluid temperature with linear heat source, thermal radiation, and volume fraction of silver nanoparticles?
- How sensitive are the physical quantities with spherical and non-spherical nanoparticles?

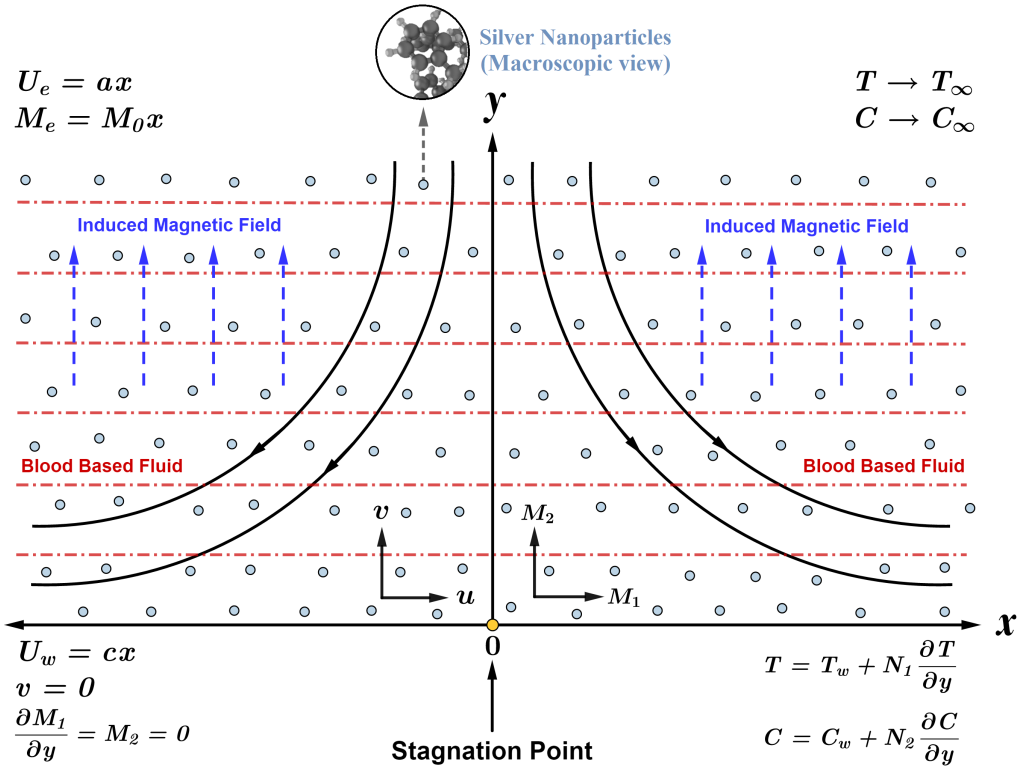

Figure 5.1: Geometrical Frame

5.2 Mathematical Frame

Two-dimensional steady incompressible stagnation point flow over a linearly elongating sheet (see Figure 5.1) is considered under the ensuing assumptions:

- The expanding sheet is positioned along x axis and blood-based silver nanofluid occupies the region $y > 0$.

- $U_w(x) = cx$ and $U_e(x) = ax$ correspond to the velocity of the lengthening sheet and the free stream, respectively.
- Induced magnetic field vector, $M = (M_1, M_2)$ is considered with M_1 & M_2 being the magnetic integrants along x and y direction, respectively.
- Chemical reaction, linear heat source, thermal radiation, and nanoparticle shape (sphere, cylinder, platelet, and blade) effects are incorporated.
- Thermal and solutal slip effects are also considered.

Following the aforementioned assumptions, the governing equations are written as (see El-Aziz & Afify, 2018; Barik et al., 2020):

$$\frac{\partial u}{\partial x} + \frac{\partial v}{\partial y} = 0 \tag{5.2.1}$$

$$\frac{\partial M_1}{\partial x} + \frac{\partial M_2}{\partial y} = 0 \tag{5.2.2}$$

$$u\frac{\partial u}{\partial x} + v\frac{\partial u}{\partial y} - \frac{\mu_e}{4\pi\rho_{nf}}\left(M_1\frac{\partial M_1}{\partial x} + M_2\frac{\partial M_1}{\partial y}\right) = U_e\frac{dU_e}{dx} - \frac{\mu_e M_e}{4\pi\rho_{nf}}\frac{dM_e}{dx} + \left(\frac{\mu_{nf}}{\rho_{nf}}\right)\frac{\partial^2 u}{\partial y^2} \tag{5.2.3}$$

$$u\frac{\partial M_1}{\partial x} + v\frac{\partial M_1}{\partial y} - M_1\frac{\partial u}{\partial x} - M_2\frac{\partial u}{\partial y} = \alpha_m\frac{\partial^2 M_1}{\partial y^2} \tag{5.2.4}$$

$$u\frac{\partial T}{\partial x} + v\frac{\partial T}{\partial y} = \alpha_{nf}\frac{\partial^2 T}{\partial y^2} + \frac{q_T}{(\rho C_p)_{nf}}(T - T_\infty) - \frac{1}{(\rho C_p)_{nf}}\frac{\partial q_r}{\partial y} \tag{5.2.5}$$

$$u\frac{\partial C}{\partial x} + v\frac{\partial C}{\partial y} = D_B\frac{\partial^2 C}{\partial y^2} - k_r(C - C_\infty) \tag{5.2.6}$$

subject to the boundary conditions (see El-Aziz & Afify, 2018; Barik et al., 2020):

$$u = U_w(x) = cx,\ v = 0,\ \tfrac{\partial M_1}{\partial y} = M_2 = 0,\ T = T_w + N_1\tfrac{\partial T}{\partial y},\ C = C_w + N_2\tfrac{\partial C}{\partial y} \ \text{ at } y = 0$$

$$u \to U_e(x) = ax,\ M_1 \to M_e(x) = M_0 x,\ T \to T_\infty, C \to C_\infty \ \text{ as } y \to \infty$$

where $\alpha_m = \dfrac{1}{4\pi\mu_e\sigma_{nf}}$ represents the magnetic diffusivity.

Consider the following similarity transformations (see El-Aziz & Afify, 2018; Barik et al., 2020):

$$u = cxf\,'(\eta),\ v = -\sqrt{c\vartheta_f}f(\eta),\ M_1 = M_0 x g\,'(\eta),\ M_2 = -M_0\sqrt{\frac{\vartheta_f}{c}}g(\eta),$$

$$\eta = y\sqrt{\frac{c}{\vartheta_f}},\ \theta(\eta) = \frac{T-T_\infty}{T_w-T_0},\ \psi(\eta) = \frac{C-C_\infty}{C_w-C_0}$$

Employing the linearized Roseland approximation and the similarity transformations into Equations $(5.2.1)-(5.2.6)$, we get:

$$f\,''' = A_1\ A_2\ \left\{\ (\ f\,'\ )^2 - f\ f\,'' - \frac{\beta}{A_2}\ \left\{\ (\ g\,'\ )^2 - g\ g\,'' - 1\right\} - A^2\ \right\} \tag{5.2.7}$$

$$g\,''' = \frac{A_5}{\lambda}\ \{\ g\ f\,'' - f\ g\,''\ \} \tag{5.2.8}$$

$$\theta\,'' = \frac{-Pr\ \{\ A_3\ f\ \theta\,' + Q_T\ \theta\ \}}{A_4 + \frac{4}{3}R_d} \tag{5.2.9}$$

$$\psi\,'' = Kr\ Le\ \psi - Le\ f\ \psi\,' \tag{5.2.10}$$

subject to the boundary conditions

$$f(0) = 0, f\,'(0) = 1,\ g(0) = 0,\ g\,''(0) = 0,\ \theta(0) = 1 + T_{slip}\ \theta\,'(0),$$

$$\psi(0) = 1 + C_{slip}\ \psi\,'(0)\,,\ f\,'(\infty) \to A,\ g\,'(\infty) \to 1,\ \theta(\infty) \to 0,\ \psi(\infty) \to 0.$$

where the dimensionless parameters are given in appendix I.

The nanofluid models and nanaoparticle shape properties incorporated are given by (see Benkhedda et al., 2020):

Spherical	***Non-spherical***
$\frac{\mu_{nf}}{\mu_f} = \frac{1}{(1-\phi)^{2.5}} = \frac{1}{A_1}$	$\frac{\mu_{nf}}{\mu_f} = 1 + A_{shape}\ \phi + B_{shape}\ \phi^2 = \frac{1}{A_1}$

$$A_2 = \frac{\rho_{nf}}{\rho_f} = (1-\phi) + \phi\left(\frac{\rho_{Ag}}{\rho_f}\right)$$

$$A_3 = \frac{(\rho C_p)_{nf}}{(\rho C_p)_f} = (1-\phi) + \phi\left(\frac{(\rho C_p)_{Ag}}{(\rho C_p)_f}\right)$$

$$A_4 = \frac{k_{nf}}{k_f} = \frac{k_{Ag} + (s-1)\,k_f - (s-1)\,\phi\,(k_f - k_{Ag})}{k_{Ag} + (s-1)\,k_f + \phi\,(k_f - k_{Ag})}$$

$$A_5 = \frac{\sigma_{nf}}{\sigma_f} = 1 + \frac{3\left(\frac{\sigma_{Ag}}{\sigma_f} - 1\right)\phi}{\left(\frac{\sigma_{Ag}}{\sigma_f} + 2\right) - \left(\frac{\sigma_{Ag}}{\sigma_f} - 1\right)\phi}$$

	Sphere	***Cylinder***	***Platelet***	***Blade***
A	-	13.5	37.1	14.6
B	-	904.4	612.6	123.3
Shape factor, s	3	4.9	5.7	8.6

The physical quantities are given by (see Z. Iqbal, Azhar, & Maraj, 2017; M. I. Khan et al., 2019):

$$\text{Local drag coefficient} \quad : \quad Cf_x = \frac{\tau_\omega}{\rho_f\ (U_w)^2} = \frac{\mu_{nf}\ \left.\frac{\partial u}{\partial y}\right|_{y=0}}{\rho_f\ (U_w)^2}$$

$$\Rightarrow\ Cf_x\ Re_x^{1/2} = \frac{f\,''(0)}{A_1}$$

$$\text{Local Nusselt number} \quad : \quad Nu_x = \frac{x\ q_\omega}{k_f\ (T_w - T_\infty)} = \frac{-x\left(k_{nf}\ \frac{\partial T}{\partial y} - q_r\right)\Big|_{y=0}}{k_f\ (T_w - T_\infty)}$$

$$\Rightarrow\ Nu_x\ Re_x^{-\ 1/2} = -\left(A_4 + \frac{4}{3}R_d\right)\ \theta\,'(0)$$

$$\text{Local Sherwood number} \quad : \quad Sh_x = \frac{x\ q_m}{D_B\ (C_w - C_0)} = \frac{-x\ D_B\ \frac{\partial C}{\partial y}\Big|_{y=0}}{D_B\ (C_w - C_0)}$$

$$\Rightarrow\ Sh_x\ Re_x^{-\ 1/2} = -\ \psi\,'(0)$$

where $Re_x = \frac{xU_w}{\vartheta_f}$ is the local Reynold's number.

5.3 Numerical Frame & Validation

Equations (5.2.7) - (5.2.10) together with the boundary conditions are numerically resolved in MATLAB employing the adaptive Runge-Kutta method (for solving) and Newton Raphson (for shooting). Shooting technique involves converting the boundary value problem into an initial value problem and then estimating the unknowns using the far-field boundary conditions. For this, initially assume:

$$\Gamma_1 = f,\quad \Gamma_2 = f\,',\quad \Gamma_3 = f\,'',\quad \Gamma_3{}' = f\,''',\ \Gamma_4 = g,\quad \Gamma_5 = g\,',\ \Gamma_6 = g\,'',$$
$$\Gamma_6{}' = g\,''',\quad \Gamma_7 = \theta\ ,\quad \Gamma_8 = \theta\,',\quad \Gamma_8{}' = \theta\,''\ ,\quad \Gamma_9 = \psi,\ \Gamma_{10} = \psi\,',\quad \Gamma_{10}{}' = \psi\,''$$

The reduced system of the first-order ODE is given by:

$$\Gamma_1{}' = \Gamma_2\ ,\ \Gamma_2{}' = \Gamma_3\ ,$$

$$\Gamma_3{}' = A_1\ A_2\ \left\{\ (\Gamma_2)^2 - \Gamma_1\ \Gamma_3 - \frac{\beta}{A_2}\ \left\{(\Gamma_5)^2 - \Gamma_4\ \Gamma_6 - 1\right\} - A^2\ \right\},$$

$$\Gamma_4{}' = \Gamma_5\ ,\ \Gamma_5{}' = \Gamma_6\ ,$$

$$\Gamma_6{}' = \frac{A_5}{\lambda}\ \{\ \Gamma_4\ \Gamma_3 - \Gamma_1\ \Gamma_6\ \}\ ,$$

$$\Gamma_7{}' = \Gamma_8\ ,\ \Gamma_8{}' = \frac{-Pr\ \{\ A_3\ \Gamma_1\ \Gamma_8 + Q_T\ \Gamma_7\ \}}{A_4 + \frac{4}{3}R_d}\ ,$$

$$\Gamma_9{}' = \Gamma_{10}\ ,\ \Gamma_{10}{}' = Kr\ Le\ \Gamma_9 - Le\ \Gamma_1\ \Gamma_{10}\ .$$

with

$$\Gamma_1(0) = 0\ ,\ \Gamma_2(0) = 1\ ,\ \Gamma_3(0) = \Lambda_1\ ,\ \Gamma_4(0) = 0\ ,\ \Gamma_5(0) = \Lambda_2\ ,\ \Gamma_6(0) = 0,$$
$$\Gamma_7(0) = 1 + T_{slip}\ \Lambda_3\ ,\ \Gamma_8(0) = \Lambda_3\ ,\ \Gamma_9(0) = 1 + C_{slip}\ \Lambda_4\ ,\ \Gamma_{10}(0) = \Lambda_4.$$

where Λ_1 , Λ_2 , Λ_3 & Λ_4 are estimated using the Newton Raphson method with a suitable initial guess.

Validity of the code for the current problem has been adjudged through a restrictive correspondence of the present work with prior published works of Hayat et al., 2015, 2016; Iqbal, Azhar, et al., 2017 (showcased in Table 5.1) and a commendable agreement is noted.

5.4 Results & Discussion

The consequence of influential parameters on velocity ($f'(\eta)$), concentration ($\psi(\eta)$), temperature ($\theta(\eta)$), induced magnetic field ($g'(\eta)$) profiles and physical quantities are illustrated via Figures 5.2 - 5.25. Prandtl number (Pr) and infinity are fixed at 21 and 5, respectively. Thermophysical properties of base fluid (blood) and silver (nanoparticle) are showcased in Table 5.2.

Figure 5.2 elucidates the positive impact of the stretching parameter (A) on $f'(\eta)$ meaning that an augmentation in stretching parameter results in the escalation of $f'(\eta)$. Figure 5.3 describes the deviations in $f'(\eta)$ with β (magnetic parameter). An increase in β tends to increase $f'(\eta)$. Figure 5.4 bespeaks the deviations in $f'(\eta)$ with respect to ϕ (nanoparticle volume fraction). It can be observed that $f'(\eta)$ decreases for augmenting ϕ values. This can be physically associated with the fact that ascending ϕ values increases the nanofluid viscosity which in turn decreases the nanofluid velocity. The nanoparticle shape effect on velocity profile is depicted in Figure 5.5. The highest nanofluid velocity profile is exhibited by cylinder-shaped silver nanoparticles followed by platelet, blade, and spherical-shaped nanoparticles, respectively.

Figures 5.6 & 5.7 elucidate the parallel effect of β & ϕ with the differing nanoparticle shapes on $Cf_x\ Re_x^{1/2}$. It is perceived that $Cf_x\ Re_x^{1/2}$ is a decreasing function of ϕ and an increasing function of β. Further, it can be observed that the drag coefficient is highest for spherical-shaped silver nanoparticles and least for cylindrically shaped silver nanoparticles.

Table 5.1: Comparison of drag coefficient $\left(Cf_x Re_x^{1/2}\right)$ for different A values between the present study and the works of Iqbal, Azhar, et al., 2017 and Hayat et al., 2015, 2016 when $\phi = \beta = 0$

A	$\boldsymbol{Cf_x Re_x^{1/2}}$			
	Iqbal et al., 2017	**Hayat et al., 2015**	**Hayat et al., 2016**	**Present study**
0.1	-0.969386	-0.96939	-0.96937	-0.9693861
0.2	-0.918107	-0.91811	-0.91813	-0.9181071
0.5	-0.667263	-0.66726	-0.66723	-0.6672637
0.7	-0.433475	-0.43346	-0.43345	-0.4334756
0.8	-0.299388	-0.29929	-0.29921	-0.2993888
0.9	-0.154716	-0.15458	-0.1545471	-0.1547167
1	0	0	0	0

Table 5.2: Thermophysical properties of blood and silver

Property	**Blood (base fluid)**	**Silver (nanoparticle)**
$\boldsymbol{\rho}$	1063	10490
$\boldsymbol{C_p}$	3594	235
$\boldsymbol{k}$	0.492	429
$\boldsymbol{\sigma}$	0.8	6.3×10^7

Table 5.3: Variation in $Sh_x\ Re_x^{-\ 1/2}$ when $A = 0.5$, $\beta = 0.1$, $\lambda = 0.5$ & $\phi = 0.1$

Kr	**Le**	$\mathbf{C_{slip}}$	$\mathbf{Sh_x\ Re_x^{-1/2}}$			
			Sphere	***Cylinder***	***Platelet***	***Blade***
1.5	0.3	0.3	0.6166	0.6263	0.6261	0.6217
2.0	0.3	0.3	0.6773	0.6852	0.6850	0.6815
2.5	0.3	0.3	0.7298	0.7363	0.7362	0.7333
2.0	0.2	0.3	0.5737	0.5808	0.5807	0.5774
2.0	0.3	0.3	0.6773	0.6852	0.6850	0.6815
2.0	0.4	0.3	0.7594	0.7675	0.7674	0.7638
2.0	0.3	0.2	0.7265	0.7355	0.7354	0.7313
2.0	0.3	0.3	0.6773	0.6852	0.6850	0.6815
2.0	0.3	0.4	0.6343	0.6412	0.6411	0.6380

Figure 5.8 displays the negative impact of A on $g'(\eta)$ whereas Figure 5.9 displays the positive impact of β on $g'(\eta)$. Figure 5.10 explains the mixed effect of λ (reciprocal of magnetic Prandtl number) on $g'(\eta)$. Initially, elevating λ values decays $g'(\eta)$ and afterwards, a reversed trend is observed. The dual nature is evident from the relation that λ is inversely proportional to the momentum diffusivity. Figure 5.11 represents nanoparticle shape effect on $g'(\eta)$. The highest and lowest induced magnetic field profiles are recorded by cylindrical and spherical shaped silver nanoparticles, respectively.

The consequence of A on $\theta(\eta)$ is graphed in Figure 5.12. A decline in temperature is noted for the increasing A values. Figure 5.13 throws light into the constructive nature of ϕ on $\theta(\eta)$. Physically, the improvement in $\theta(\eta)$ is due to the increased thermal conductivity of fluid caused by the hike in nanoparticle volume fraction. In addition, the inherent nature of nanoparticles is bound to affect the temperature distribution. The influence of Q_T (linear heat source parameter) and R_d (thermal radiation parameter) on $\theta(\eta)$ is analyzed in Figures 5.14 & 5.15, respectively. Both parameters tend to increase $\theta(\eta)$. This can be associated with the fact that an increase in Q_T & R_d supplies supplemental energy to the system which triggers a surge in $\theta(\eta)$. Biologically, the increase in temperature profiles due to augmenting nanoparticle volume fraction, linear heat source, and thermal radiation unveils that the nanofluid can be used for killing tumors or cancerous cells.

The effect of T_{slip} (thermal slip parameter) is analyzed with the aid of Figure 5.16. It is noted that augmenting T_{slip} values lead to a decrease in $\theta(\eta)$. Augmentation in the thermal slip parameter reduces the sensitivity of the fluid flow within the boundary layer, which reduces the amount of heat produced and thereby reduces the temperature. The impact of nanoparticle shape on $\theta(\eta)$ is explained in Figure 5.17. The blade-shaped silver nanoparticles contribute the most towards $\theta(\eta)$ and cylinder-shaped silver nanoparticles contribute the least towards $\theta(\eta)$.

The parallel effect of ϕ, Q_T, R_d & T_{slip} with the differing nanoparticle shapes on $Nu_x\ Re_x^{-1/2}$ is elucidated in Figure 5.18 - 5.21. It is seen that ϕ & R_d promotes $Nu_x\ Re_x^{-1/2}$ whereas Q_T & T_{slip} demotes $Nu_x\ Re_x^{-1/2}$. A significant rise in the heat transfer rate is showcased by the blade-shaped silver nanoparticles followed by platelet, cylinder, and spherical-shaped nanoparticles, respectively.

Variation in $\psi(\eta)$ for differing A values is demonstrated in Figure 5.22 and it is perceived that A has a negative effect on $\psi(\eta)$. Figure 5.23 elucidates the effect of Le (Lewis number) on $\psi(\eta)$. $\psi(\eta)$ decreases with augmenting Le values. Figure 5.24 explains the negative impact of Kr (chemical reaction parameter) on $\psi(\eta)$. This can be associated with the fact that augmenting Kr values eats up the nanoparticle which decreases $\psi(\eta)$. Biologically, consumption of more nanoparticles is directly proportional to improved medication and hyperthermia. The impact of C_{slip} (solutal slip parameter) on $\psi(\eta)$ is graphed in Figure 5.25. It is seen that increasing C_{slip} values help in decreasing $\psi(\eta)$.

The consequence of pertinent parameters on $Sh_x\ Re_x^{-\ 1/2}$ is explained in Table 5.3. It is perceived that Kr & Le have a positive impact on $Sh_x\ Re_x^{-\ 1/2}$ and C_{slip} descends $Sh_x\ Re_x^{-\ 1/2}$. In addition, it is observed that the cylinder-shaped silver nanoparticles offer the highest $Sh_x\ Re_x^{-\ 1/2}$ value.

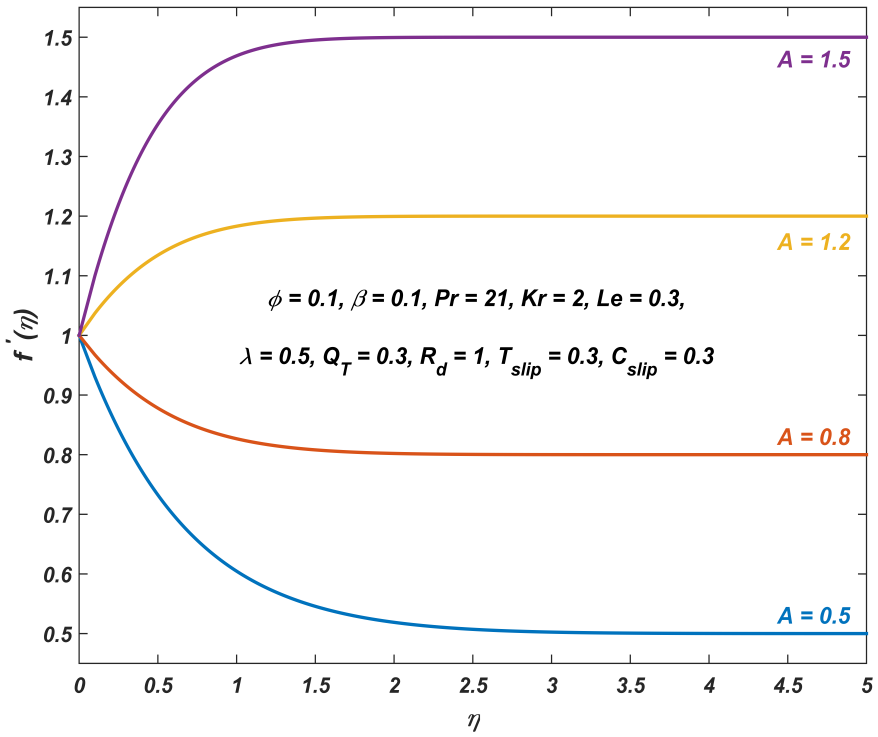

Figure 5.2: $f'(\eta)$ for differing A values

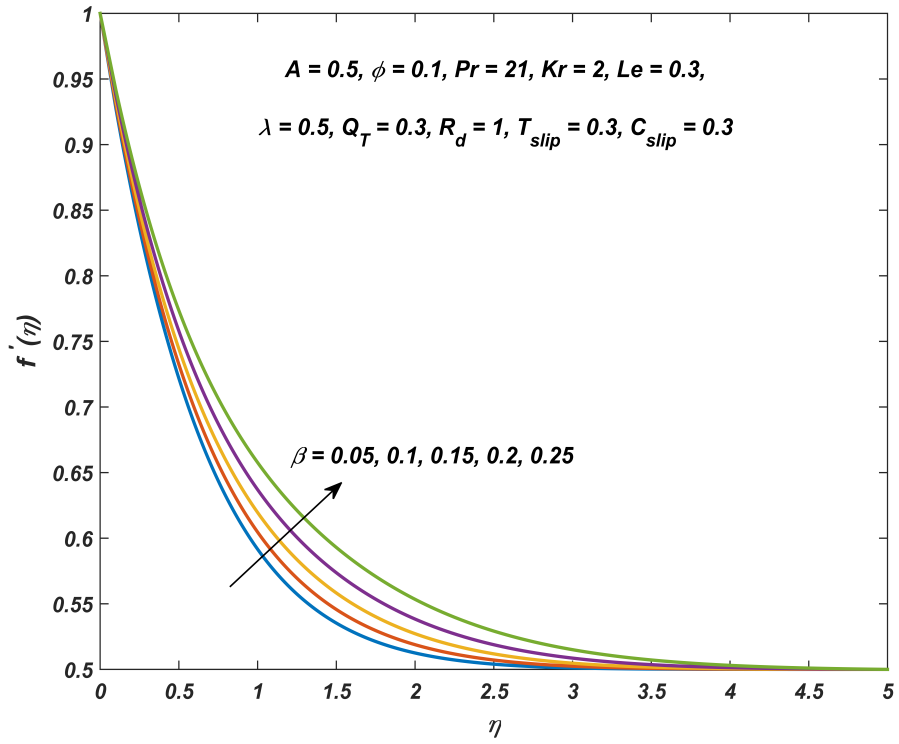

Figure 5.3: $f'(\eta)$ for differing β values

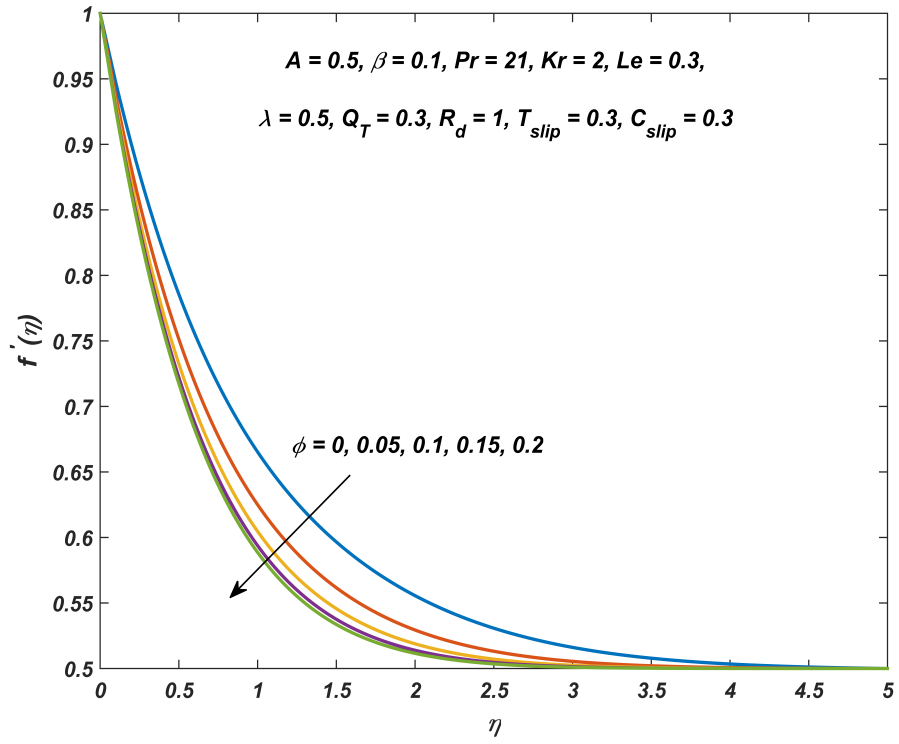

Figure 5.4: $f'(\eta)$ for differing ϕ values

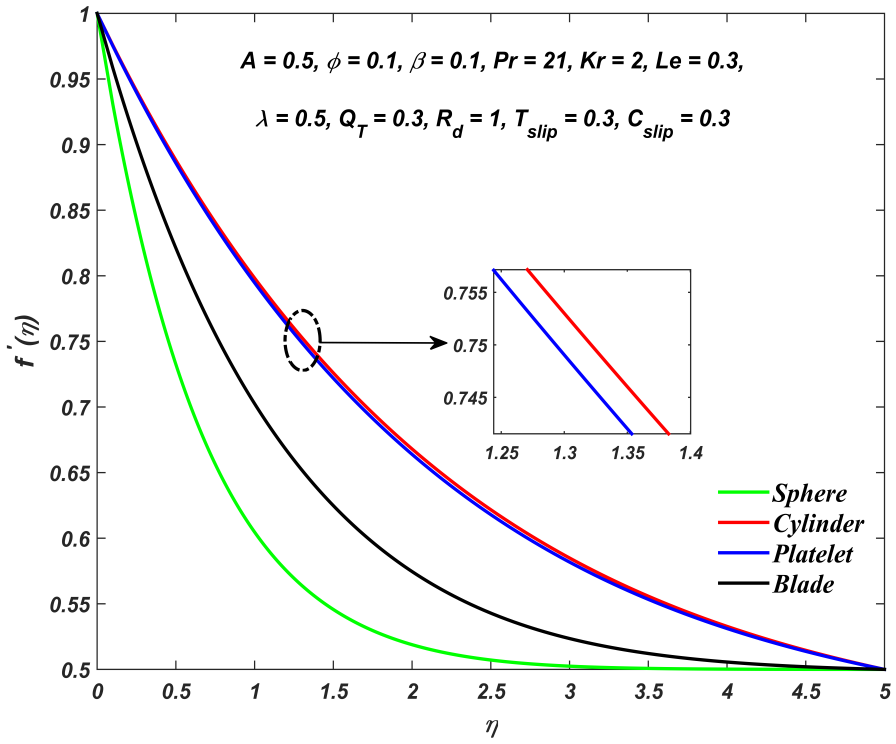

Figure 5.5: $f'(\eta)$ for differing nanoparticle shapes

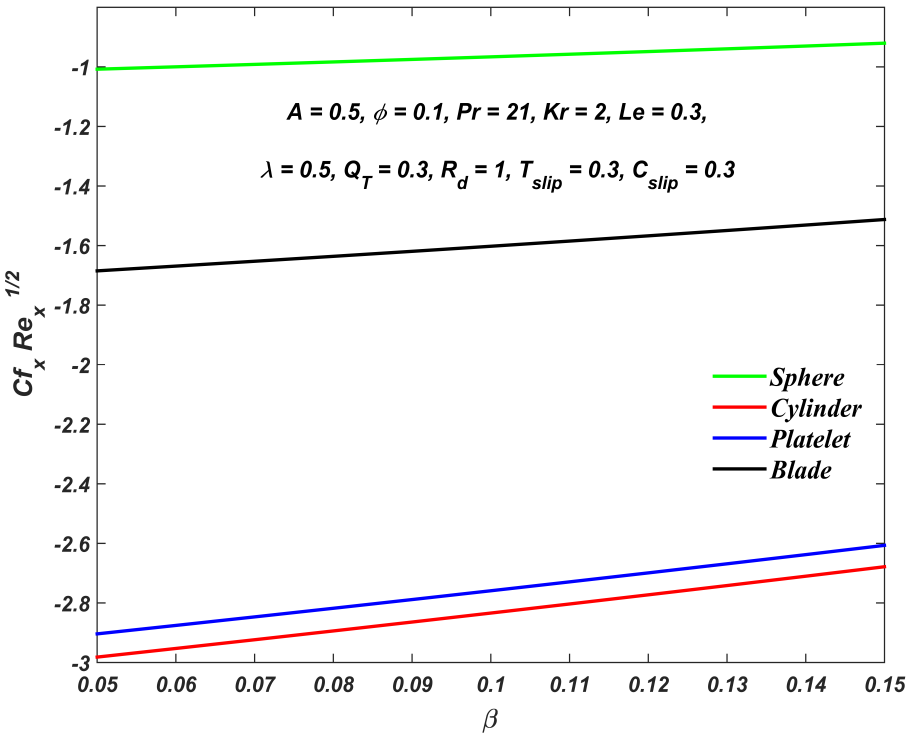

Figure 5.6: $Cf_x\ Re_x^{1/2}$ for differing nanoparticle shapes β values

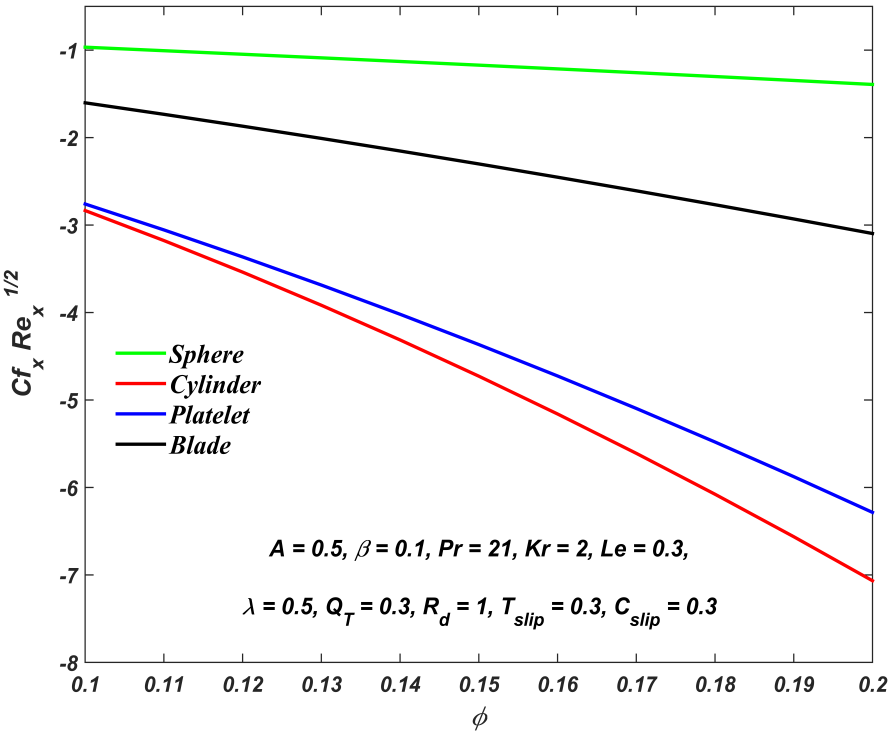

Figure 5.7: $Cf_x\ Re_x^{1/2}$ for differing nanoparticle shapes ϕ values

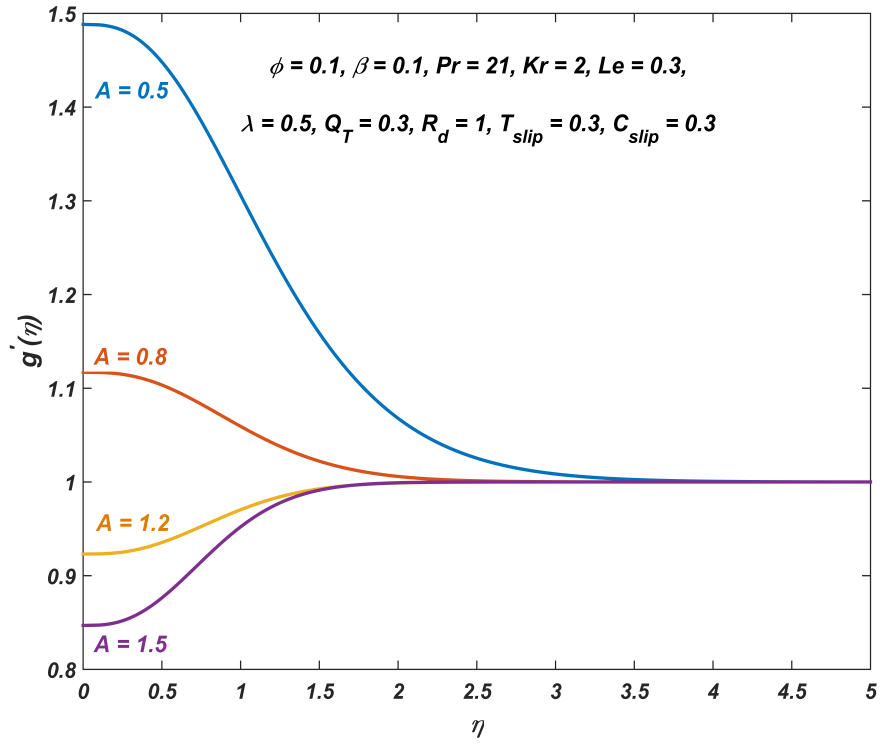

Figure 5.8: $g'(\eta)$ for differing A values

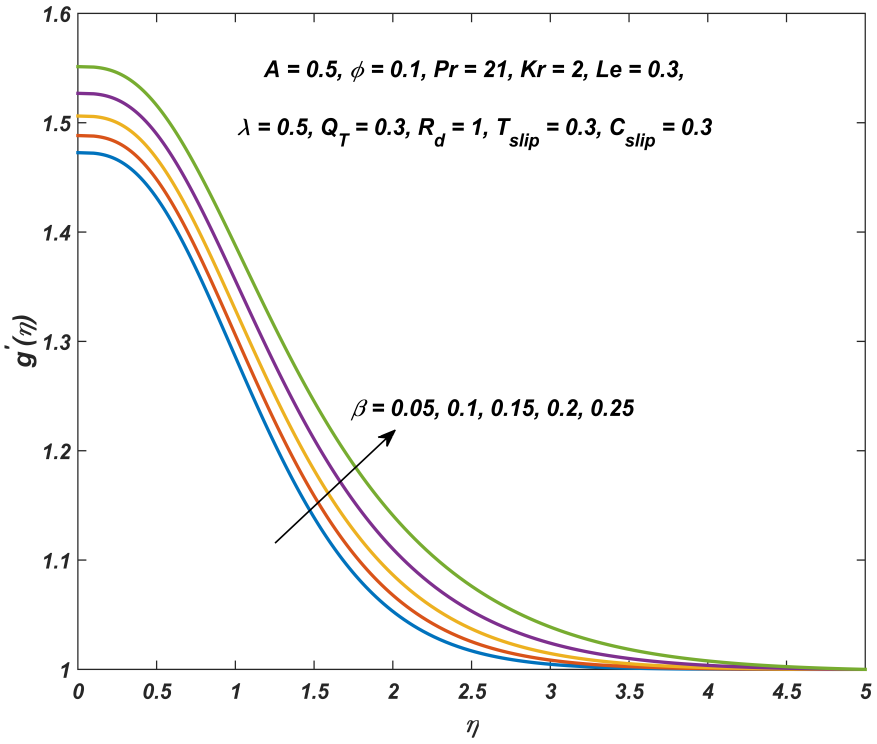

Figure 5.9: $g'(\eta)$ for differing β values

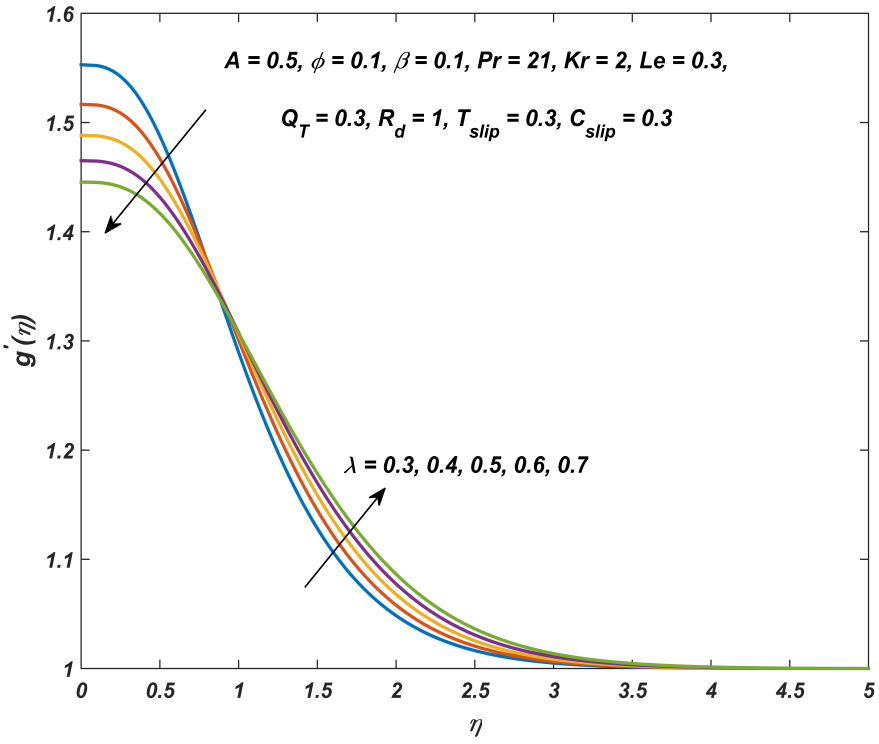

Figure 5.10: $g'(\eta)$ for differing λ values

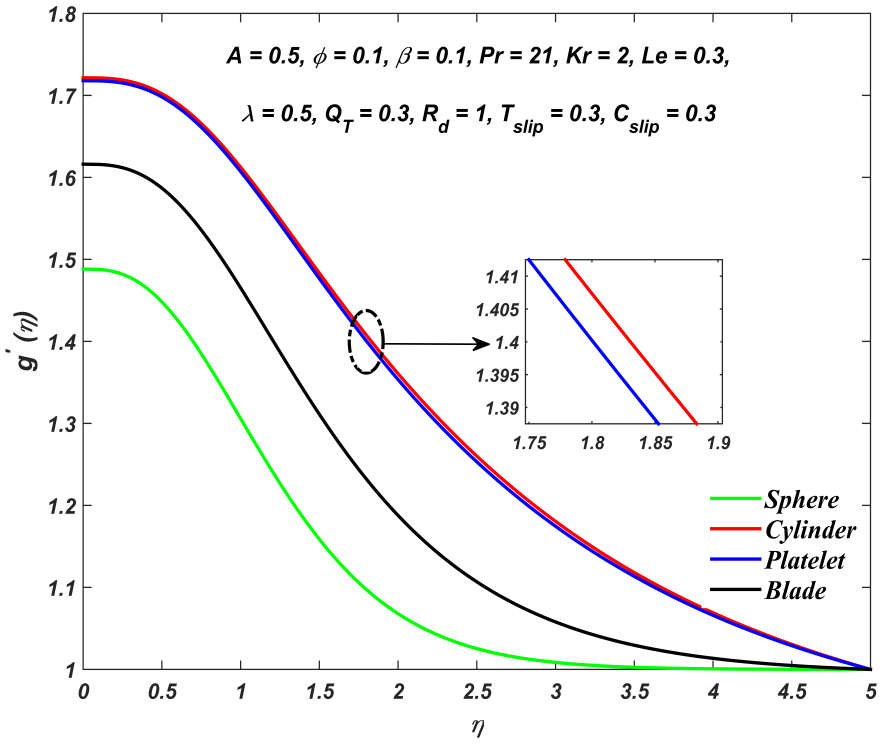

Figure 5.11: $g'(\eta)$ for differing nanoparticle shapes

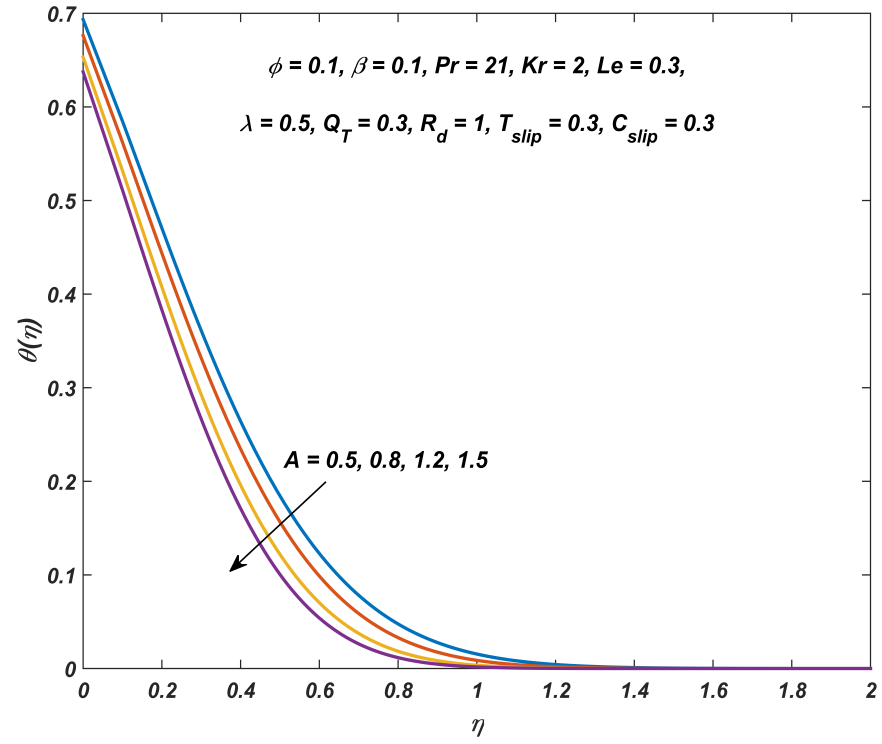

Figure 5.12: $\theta(\eta)$ for differing A values

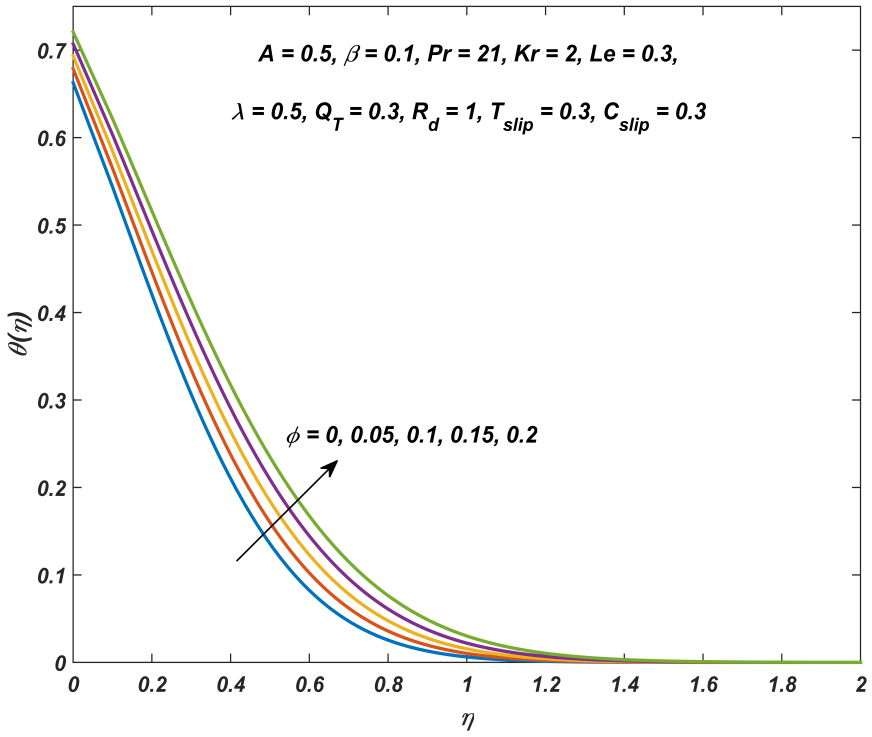

Figure 5.13: $\theta(\eta)$ for differing ϕ values

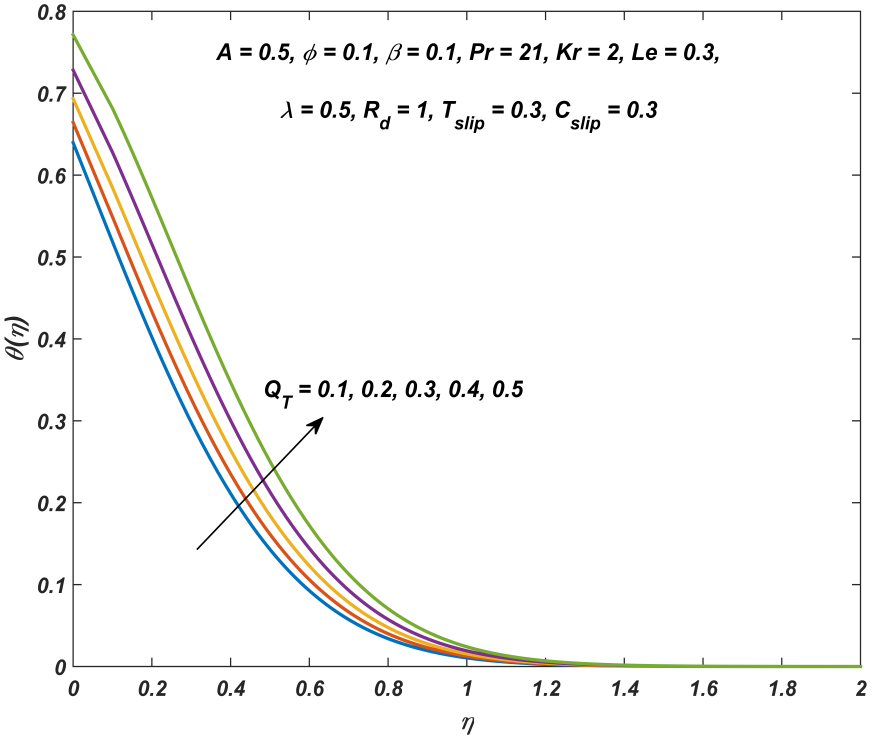

Figure 5.14: $\theta(\eta)$ for differing Q_T values

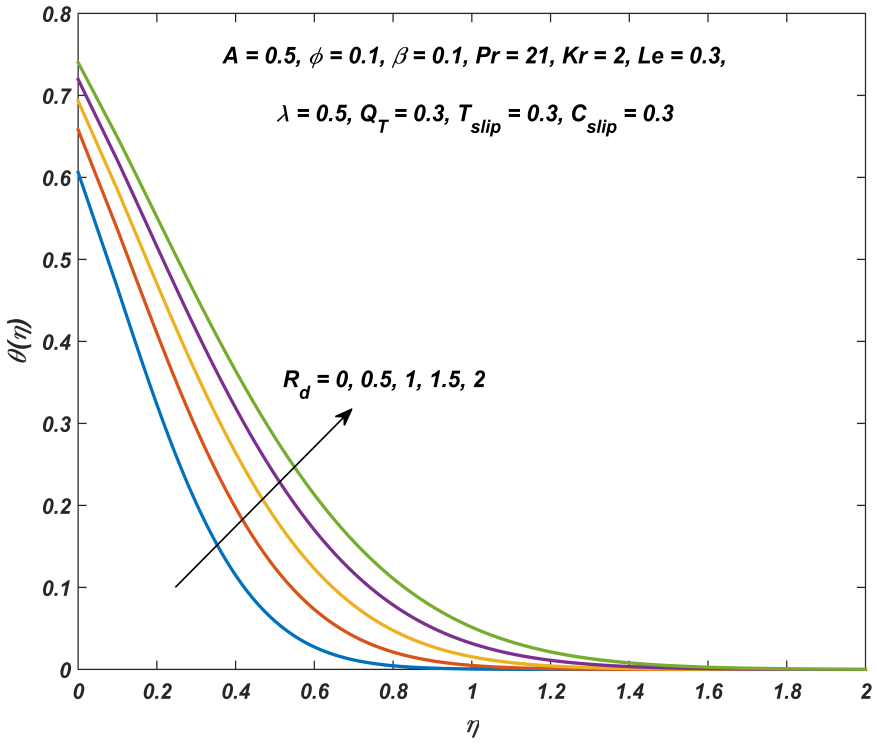

Figure 5.15: $\theta(\eta)$ for differing R_d values

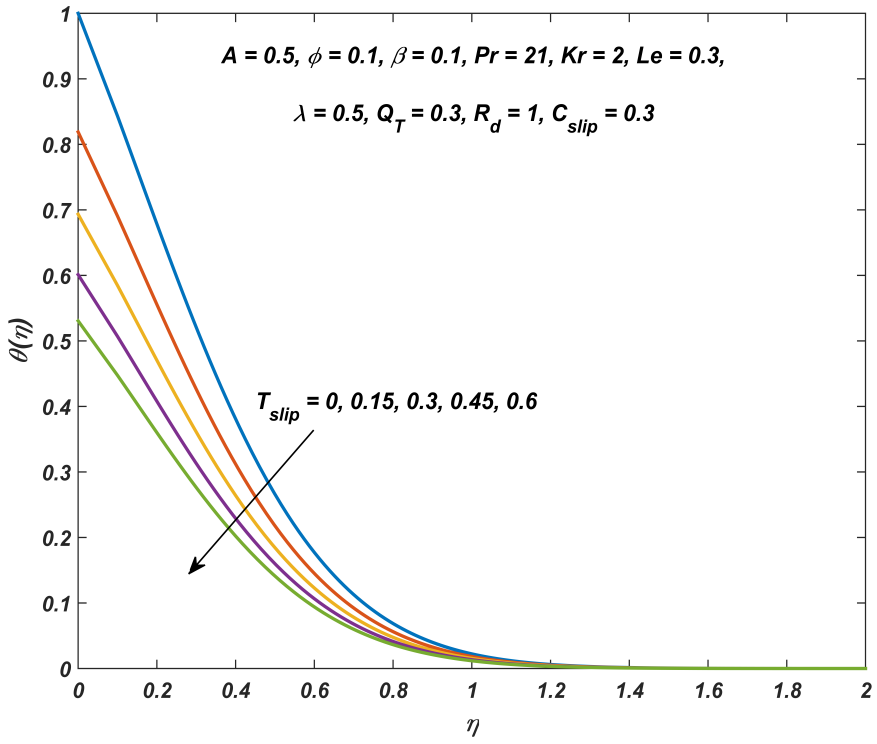

Figure 5.16: $\theta(\eta)$ for differing T_{slip} values

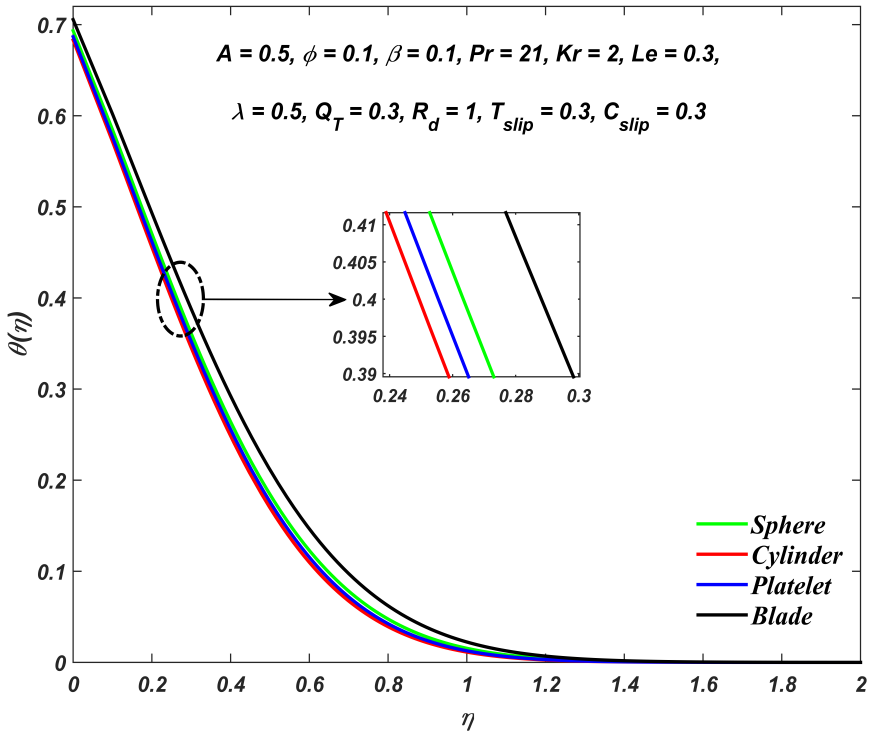

Figure 5.17: $\theta(\eta)$ for differing nanoparticle shapes

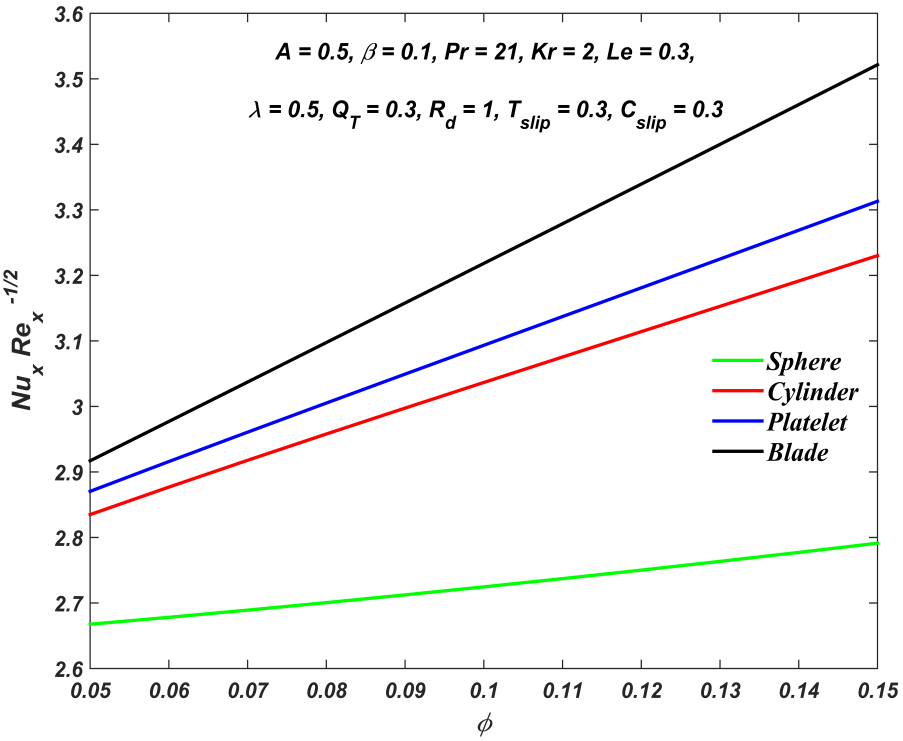

Figure 5.18: $Nu_x Re_x^{-1/2}$ for differing nanoparticle shapes and ϕ values

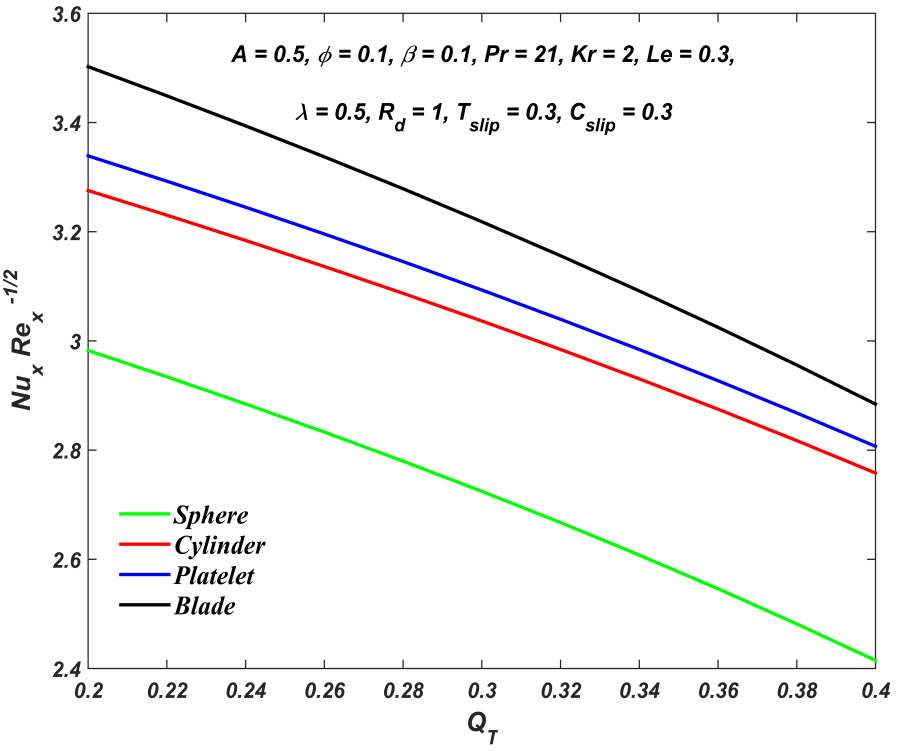

Figure 5.19: $Nu_x Re_x^{-1/2}$ for differing nanoparticle shapes and Q_T values

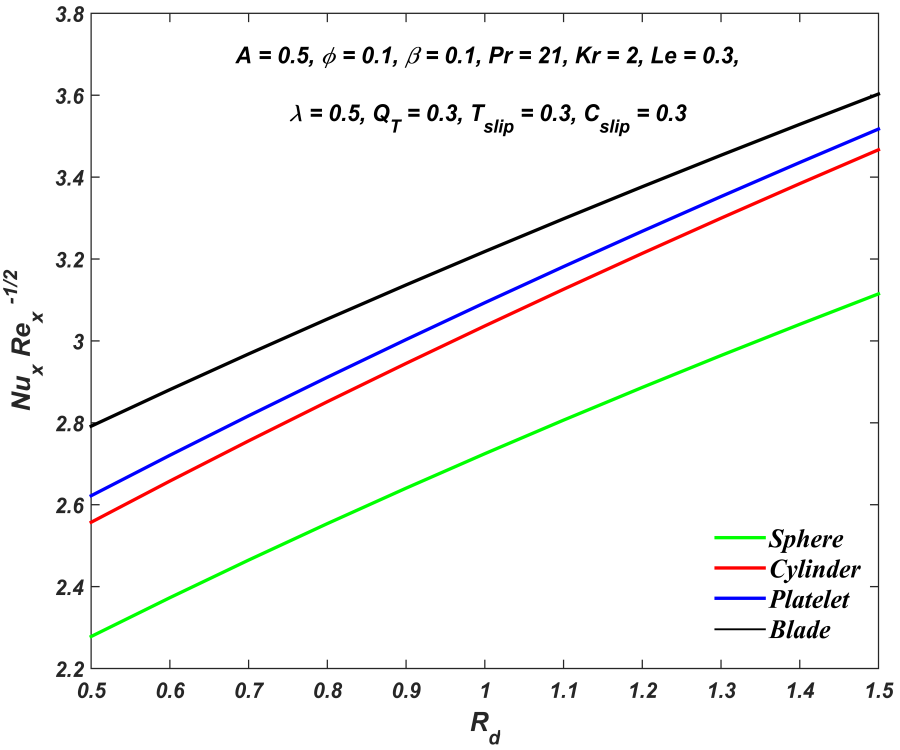

Figure 5.20: $Nu_x Re_x^{-1/2}$ for differing nanoparticle shapes and R_d values

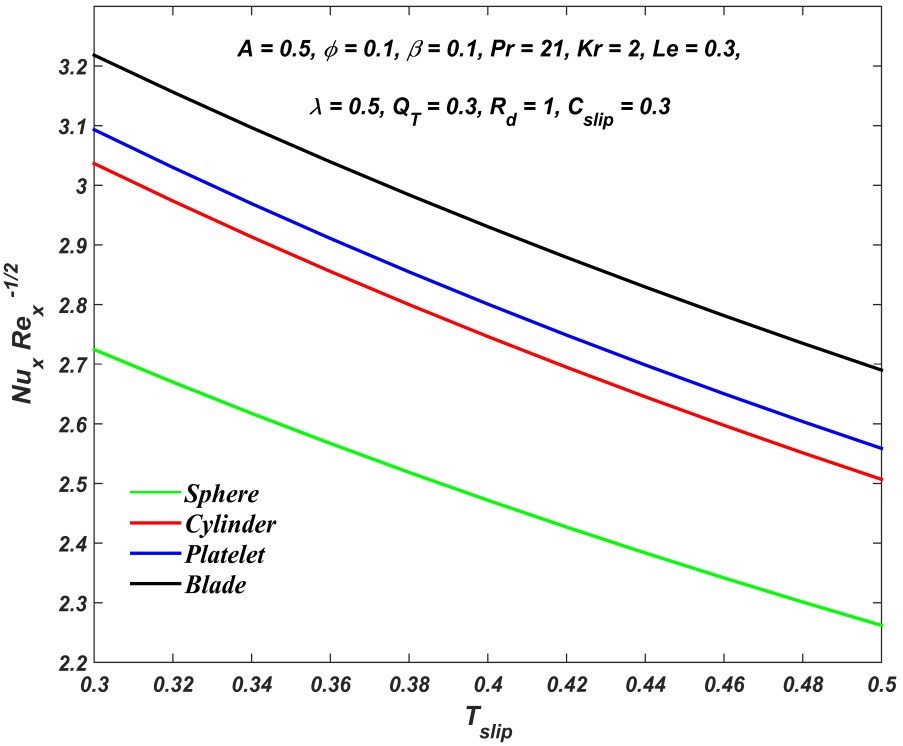

Figure 5.21: $Nu_x Re_x^{-1/2}$ for differing nanoparticle shapes and T_{slip} values

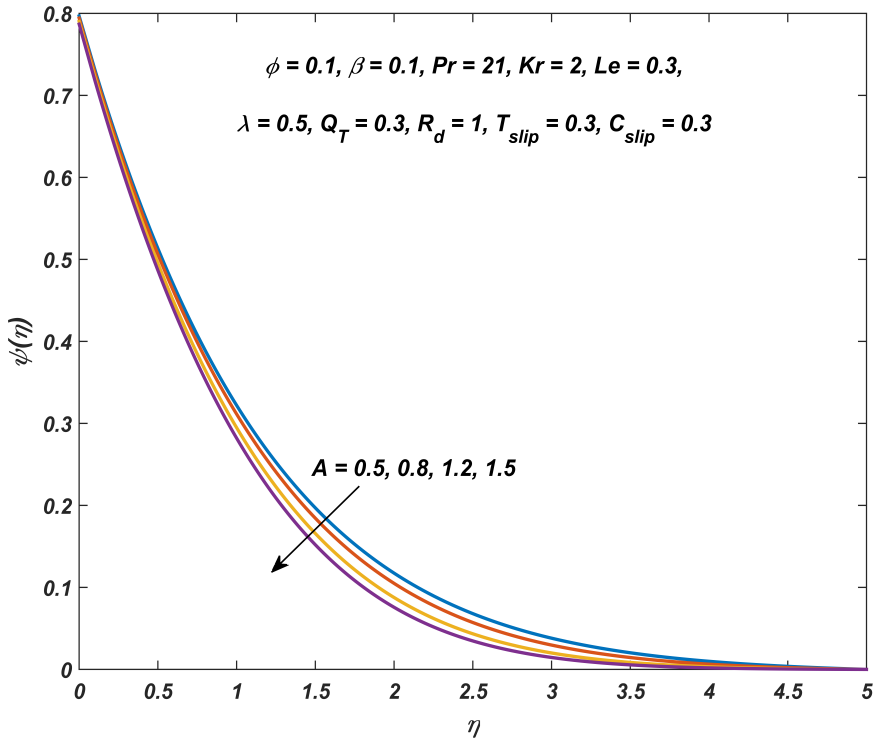

Figure 5.22: $\psi(\eta)$ for differing A values

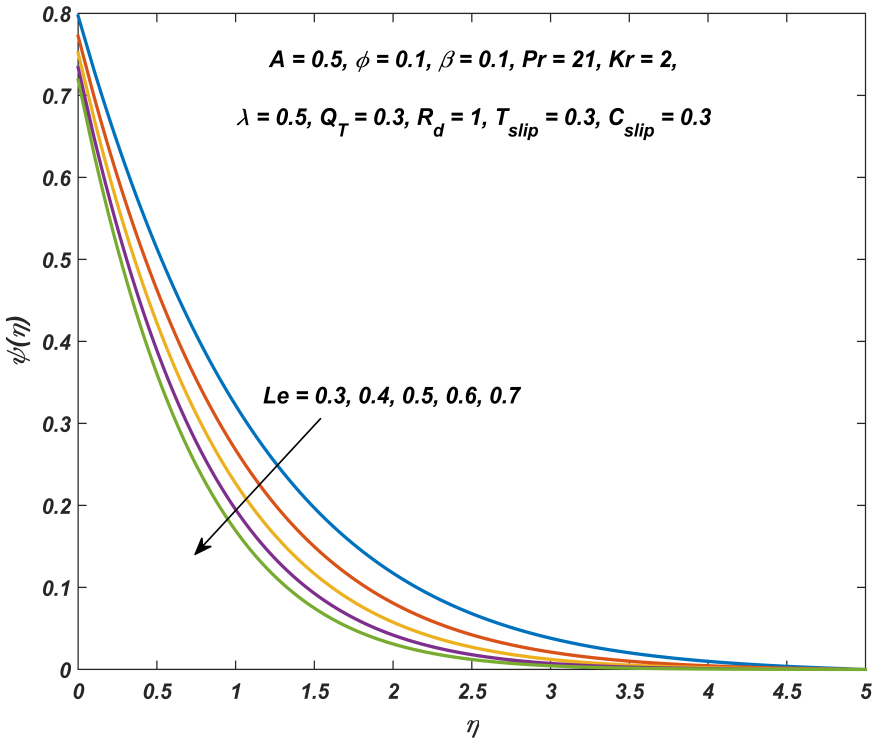

Figure 5.23: $\psi(\eta)$ for differing Le values

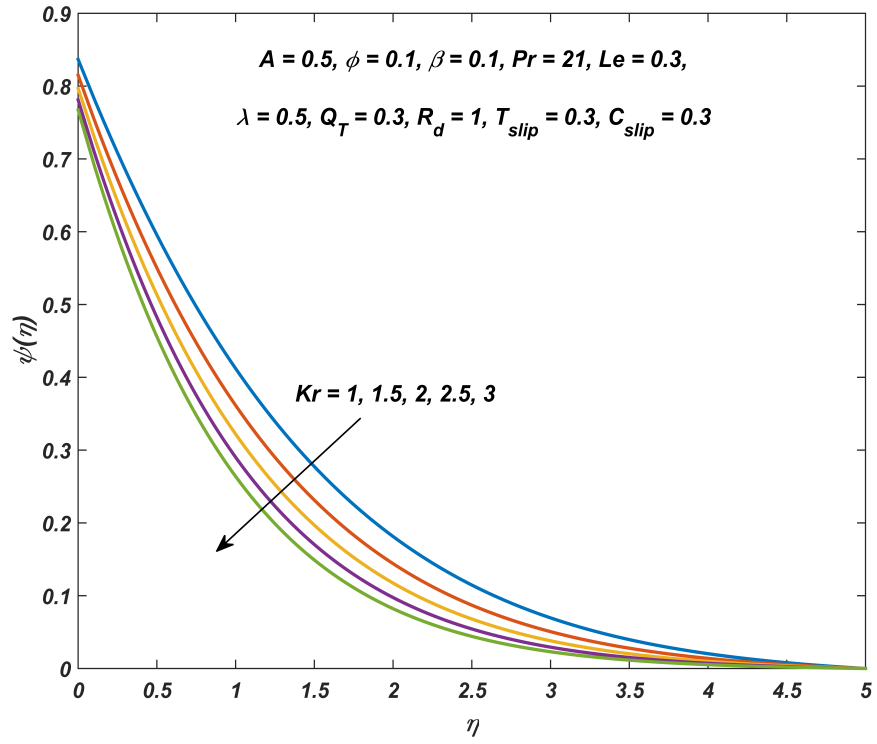

Figure 5.24: $\psi(\eta)$ for differing Kr values

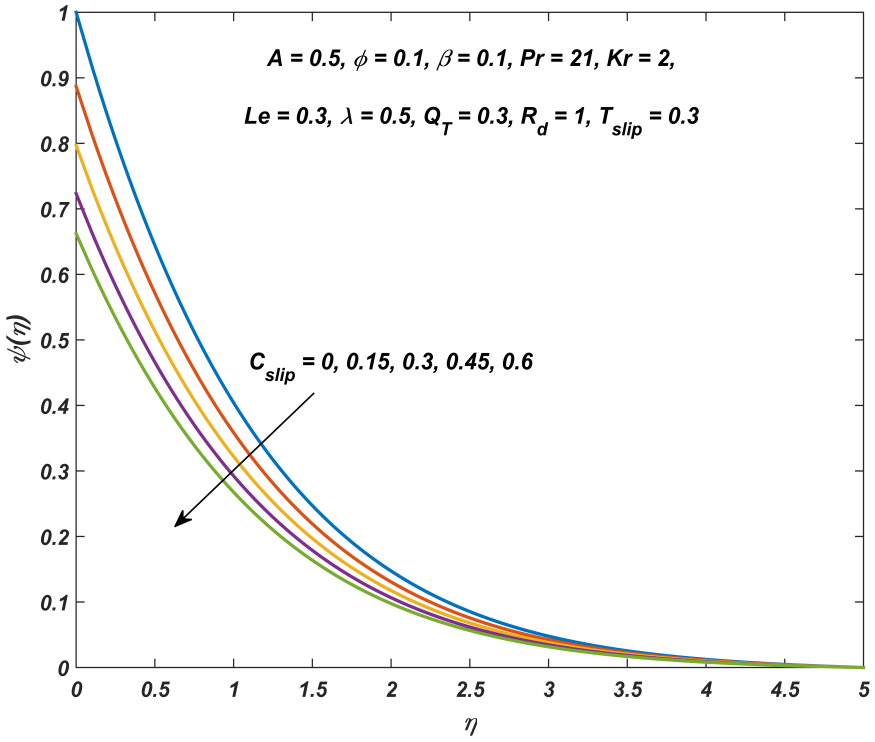

Figure 5.25: $\psi(\eta)$ for differing C_{slip} values

5.5 Conclusion

The influence of thermal and solutal slip on the stagnation point flow of blood-based silver nanomaterial in the presence of an induced magnetic field has been examined. The significance of spherical and non-spherical silver nanoparticles on the flow profiles and physical quantities has been analyzed. The key points drawn from the study are:

- Nanofluid temperature and nanofluid concentration reduce with increasing values of thermal slip and concentration slip parameters, respectively.
- Velocity and induced magnetic field profiles are least affected by spherical-shaped silver nanoparticles and highly affected by cylinder-shaped silver nanoparticles. Blade shaped silver nanoparticles contribute the most whereas cylinder-shaped silver nanoparticles contribute the least towards the nanofluid temperature.
- Nanofluid temperature ascends with augmenting linear heat source, thermal

radiation parameter, and volume fraction of silver nanoparticles.

- Blade shaped silver nanoparticles offer an increased heat transfer rate over the other nanoparticle shapes and cylinder-shaped silver nanoparticles exhibit the highest mass transfer rate. A significant rise in the surface drag is brought out by the spherical-shaped silver nanoparticles followed by blade, platelet, and cylinder-shaped nanoparticles.

Appendix I: Non-dimensional qunatities

$A = \frac{a}{c}$	Stretching parameter
$\beta = \frac{\mu_e}{4\pi\rho_f}\left(\frac{M_0}{c}\right)^2$	Magnetic parameter
$\lambda = \frac{1}{4\pi\mu_e\sigma_f\vartheta_f}$	Reciprocal of magnetic Prandtl number
$Pr = \frac{(\mu C_p)_f}{k_f} = \frac{\vartheta_f}{\alpha_f}$	Prandtl number
$Kr = \frac{k_r}{c}$	Chemical reaction parameter
$R_d = \frac{4\sigma^* {T_\infty}^3}{k^* k_f}$	Thermal radiation parameter
$Le = \frac{\vartheta_f}{D_B}$	Lewis number
$Q_T = \frac{q_T}{c\,(\rho C_p)_f}$	Linear heat source parameter
$T_{slip} = N_1\sqrt{\frac{c}{\vartheta_f}}$	Thermal slip parameter
$C_{slip} = N_2\sqrt{\frac{c}{\vartheta_f}}$	Solutal slip parameter

Appendix II: Nomenclature

a, c	Dimensional constants	q_T	Heat source coefficient
u, v	Velocity components	M_0	Uniform magnetic field at infinity
q_r	Radiative heat flux	T_∞	Ambient fluid temperature
N_1	Temperature slip factor	N_2	Concentration slip factor
C	Fluid concentration	k^*	Mean absorption coefficient
T	Fluid temperature	Q_T	Linear heat source
x, y	Cartesian coordinates	C_w	Nanoparticle concentration near wall
T_w	Wall fluid temperature	C_∞	Ambient nanoparticle concentration
C_p	Specific heat	Cf_x	Local drag coefficient
k_r	Reaction rate constant	Nu_x	Local Nusselt number
Sh_x	Local Sherwood number	R_d	Thermal radiation parameter
σ	Electrical conductivity	M_e	Magnetic field at free stream
η	Dimensionless variable	D_B	Mass diffusivity
ϑ	Kinematic viscosity	σ^*	Stefan- Boltzmann constant
k	Thermal conductivity	μ_e	Magnetic permeability
ρ	Fluid density	λ	Reciprocal of magnetic Prandtl number
β	Magnetic parameter	ϕ	Nanoparticle volume fraction
α_m	Magnetic diffusivity	α	Thermal diffusivity